Journal of Power Sources 438 (2019) 227011

Contents lists available at ScienceDirect

Journal of Power Sources

journal homepage: www.elsevier.com/locate/jpowsour

Selecting a suitable battery technology for the photovoltaic battery integrated module

Victor Vega-Garita [a,b,*], Ali Hanif [a], Nishant Narayan [a], Laura Ramirez-Elizondo [a], Pavol Bauer [a]

[a] DC Systems, Energy Conversion and Storage at Delft University of Technology, P.O. Box 5031, 2600, GA, Delft, Netherlands
[b] Electrical Engineering Department at University of Costa Rica, 11501-2060, UCR, San Pedro, San Jose, Costa Rica

HIGHLIGHTS

- An application-based methodology allows for the selection of a suitable battery. .
- High temperature results in faster degradation than the different current profiles.
- The $LiFePO_4$ cell is the most suitable battery for the *PV-battery Integrated Module*.

ARTICLE INFO

Keywords:
Battery selection
PV-Battery integration
Li-ion
Testing
Aging

ABSTRACT

The use of batteries is indispensable in stand-alone photovoltaic (PV) systems, and the physical integration of a battery pack and a PV panel in one device enables this concept while easing the installation and system scaling. However, the influence of high temperatures is one of the main challenges of placing a solar panel close to a battery pack. Therefore, this paper aims to select a suitable battery technology considering the temperature of operation and the expected current profiles. The methodology for battery selection is composed of a literature review, an integrated model, the design of an application-based testing, and the execution of the aging test. The integrated model was employed to choose among the battery technologies, and to design a testing procedure that simulated the operational conditions of the *PV-battery Integrated Module* (*PBIM*). Two Li-ion pouch cells were tested at two representative temperatures while applying various charging/discharging profiles. After the testing, the $LiFePO_4$ (LFP) cells showed better performance when compared to $LiCoO_2$ batteries (LCO), where for instance, the LCO cells capacity tested at 45°C, faded 2,45% more than the LFP cells at the same testing conditions. Therefore, LFP cells are selected as a suitable option to be part of the *PBIM*.

1. Introduction

The use of renewable energy has been identified as an unavoidable mitigation action to tackle global warming [1]. For this reason, and due to the falling in prices, photovoltaic (PV) energy has experienced a cumulative average annual growth of 49% between 2003 and 2013 in installed capacity [2]. However, with an electricity grid more and more dependent on renewable energy, the need for energy storage devices revitalizes. Energy storage devices accumulate the excess energy, if there is energy surplus, or delivers energy in times of lack of generation.

Among the different energy storage alternatives, electrochemical cells — or batteries — in combination with PV panels has been intensively explored for PV-battery systems. They normally consist of a PV panel placed outside and battery bank located indoors. However, a new concept in which the battery and PV panel are combined in the same device has been introduced in the past [3,4]. In these approaches, challenges such as thermal management and influence of high temperature on aging have been identified [5]. The thermal management has been studied previously in Ref. [6], where an optimum design can keep the battery pack operating in a safe temperature range for the *PV-battery Integrated Module* (*PBIM*). Nevertheless, according to the tested prototype of the *PBIM* in Ref. [7], the battery pack still operates at higher temperatures when compared to a systems where the batteries are placed indoors in an almost constant ambient temperature. Therefore, it is pertinent to evaluate the impact of temperature and operating conditions on battery capacity fading for battery pack experimenting similar condition as the identified for integrated PV-battery systems, which one of the objectives in this paper.

* Corresponding author. DC Systems, Energy Conversion and Storage at Delft University of Technology, P.O. Box 5031, 2600, GA, Delft, Netherlands.
E-mail address: victor.vegagarita@ucr.ac.cr (V. Vega-Garita).

https://doi.org/10.1016/j.jpowsour.2019.227011
Received 10 May 2019; Received in revised form 26 July 2019; Accepted 12 August 2019
Available online 20 August 2019

However, before determining the impact on battery aging of the operating conditions of an integrated module, it is fundamental to choose a battery technology among the multiple options. These options have been reviewed in multiple papers such as [8,9] following qualitative approaches. In Ref. [9], the batteries available to perform auxiliary services in smart grid systems are summarized, while also correlating possible benefits and suitable battery technologies per application. It is difficult to chose the most appropriate battery technology just based on qualitative analysis, although they can help to distinguish between technologies and allow to identify a few options to make the studies more manageable.

For this reason, some authors have decided to develop methodologies that respond to the application of interest. For example, according to Ref. [10], Li-ion batteries are preferable to Lead-acid (LA) batteries, when considering levelised cost of electricity as the main factor for a community energy storage case study. Similarly, in Ref. [11], a general battery model that uses the datasheet provided by the manufactures was developed to compare amongst battery technologies including the particular charging/discharging patterns observed in PV-battery systems. As a consequence, a new methodology that captures the operational conditions expected by the *PV-battery Integrated Module* is necessary in order to choose a suitable battery technology.

Therefore, this paper introduces an application-based methodology for selecting a suitable battery technology in the context of a device that integrates a PV-battery system in one module. The methodology includes the steps followed for identifying battery candidates, the criteria used to design a battery testing, and finally, the selection of a battery technology based on the results of an intensive battery aging test. Finally, the operational for the battery in the *PV-battery integrated module* is determined.

1.1. Contributions

In summary, this article contributes towards.

- assessing different candidates using an integrated model that reproduces the operating conditions of the *PV-battery integrated module* and suggest the most appropriate battery technology.
- proposing an application-based testing methodology that reproduces the operational conditions of the *PBIM*.
- selecting a suitable battery technology for the *PV-battery integrated module* by performing an aging test at 45°C and room temperature (22–26°C).
- determining a battery degradation region in which the *PV-battery integrated module* is expected to operate.

2. Battery candidates

The general features of the most widely available batteries are shown in Table 1, where the electrochemical cells are categorized based on metrics such as energy and power density, cycle life, cost, efficiency, and self-discharge.

Lead-acid (LA) batteries are considered a mature technology with low self-discharge and relatively low capital cost, which are their most prominent benefits when compared to other cells. However, LA batteries suffer from low cycle life as well as low energy and power density; therefore, these batteries are bulky and heavy and not suitable for the *PBIM*, where a high volumetric energy capacity is required. Moreover, they are made of toxic and not environmentally friendly elements [12].

Nickel-cadmium (NiCd) batteries are characterized by higher energy and power density, and better cycle life than lead-acid batteries [13]. These batteries also present memory effect [14], which restricts the battery capacity according to its usage, and high values of self-discharge. Moreover, NiCd batteries are composed of the extremely toxic Cadmium adding to their disadvantages [15].

Nickel-metal hydride (NiMH) batteries are considered an improvement over the NiCd batteries, they are safer and less susceptible to memory effect issues. Additionally, they have a higher energy and power density than NiCd. Despite these advantages, the use of rare metals has resulted in an expensive alternative [14]. Also, NiMH still present problems previously experienced in the NiCd cells such as high self-discharge and low coulombic efficiencies [18].

According to Table 1, sodium-sulfur (NaS) and vanadium redox batteries (VRB) excel in terms of power density (NaS) and cycle life (VRB); however, none of these technologies are feasible for a concept as the *PBIM* for different reasons. In the case of the NaS, they are not suitable because the temperature of operation must be in the range of 300–350 °C, much higher than the expected in the integrated module [19]. When considering the VRB, this concept is discarded as they require the use of pumps, sensors, monitoring systems, and large vessels [20].

Therefore, Li-ion appears as a viable option taking into account its higher energy density than lead-acid, NiCd and NiMH batteries, as well as higher efficiencies. Additionally, the problems related to memory effect and toxic element are avoided by using Li-ion cells. However, Li-ion cells are normally more expensive than LA and NiCd and prone to self-discharge.

Among the Li-based cells, lithium-sulfur (Li–S) and solid electrolyte Li-ion batteries have not been considered in this study, although promising, because of the early stage development and prohibitive prices. Specifically, Li–S could be able to store more energy than typical Li-ion cells, but the cells have not been able to show appropriate cycle life, and the cost remains quite high even compared to Li-ion [21]. Another alternative is Li-ion solid-state cells with a polymer electrolyte, which are considered safer than conventional Li-ion cells as they do not use volatile and flammable liquid electrolytes [22]. However, this technology is not mature yet, and it is associated with low power density, high ionic resistance at room temperature, and high manufacturing cost [23].

2.1. Comparison of Li-ion cells

The most widely employed material for the cathodes is lithium cobalt oxide (LCO) [24], or $LiCoO_2$, with advantages in terms of price, specific capacity, low self-discharge, good cycling performance and high discharge voltage [25]. However, it has disadvantages such as accelerated aging at high currents [26], and low thermal stability when operating in temperatures between 100 and 150 °C [27].

The lithium nickel oxide cell (LNO), or $LiNiO_2$, has the same crystal structure and the theoretical specific capacity as the LCO. However, LNO batteries are even more thermally unstable [26]. However, partial

Table 1
Summary of available battery technologies. Based on [16,17].

Type	LA	NiCd	NiMH	Li-ion	NaS	VRB
Energy density (Wh kg^{-1})	25–50	50–60	60–120	75–200	150–240	10–30
Power density (W kg^{-1})	75–300	~200	250–1000	500–2000	150–230	80–150
Cycle life (100% DOD)	200–1000	>1500	180–2000	1000–10,000	2500–4000	>12,000
Capital cost ($/kWh)	100–300	300–600	900–3500	300–2500	300–500	150–1000
Round-trip efficiency	75–85	70–75	65–80	85–97	75–90	75–90
Self discharge	Low	High	High	Medium	–	Negligible

substitution of Co with Ni was found to be effective to reduce the cationic disorder [28]. The thermal stability can be improved by Mg doping and also adding a small amount of Al [29]. The structure then becomes $LiNi_xCo_yAl_{(1-x-y)}O_2$ (NCA), or lithium nickel cobalt aluminum oxide, which is widely used commercially; however, elevated temperatures of operation (40–70 °C) can cause fast capacity decrease rates [26].

Lithium manganese oxide ($LiMnO_2$) cells are a potentially interesting solution as they employ Mn instead of Co and Ni, lowering costs and avoiding the use of toxic materials [26]. Nonetheless, in lithium manganese oxide (LMO) cells, the change in structure during the lithium-ion extraction has a negative impact on cycle life, and Mn tends to dissolve into the electrolyte when the battery is not cycled [30]. The problem has been tackled by adding Co, and therefore, increasing the stability of the structure [31], and creating a new type of cell, the $LiNi_xCo_yMn_zO_2$ NMC. This kind of cells have a similar nominal voltage as the LCO, but it benefits from the less amount of Co used compared to LCO. The NMC cells also show appropriate cycle stability at 50 °C, although one of the significant issues of NMC is the unique voltage profile, which does not present the expected almost flat region found in cells such as $LiFePO_4$ (LFP).

Lithium iron phosphate batteries are considered as one of the more mature and stable Li-ion technologies [24], showing an excellent thermal stability and cycle life, good power capability, and it is regarded as the safest lithium-ion type concerning thermal runaway risk. Despite all of those advantages, LFP cells are characterised by its low energy density caused by an average voltage around 3.2–3.4 V [26], which is lesser than the other Li-ion technologies, except for $Li_4Ti_5O_{12}$.

Based on the previous analysis in this section, and the operational conditions of the *PBIM*, LCO and LFP are chosen as the battery candidates. NMC cells show interesting features, but their high price and the instability of the voltage makes it an unfavorable candidate. LCO and LFP provide the right balance between available Li-ion options. While LCO has low thermal stability at significantly high temperatures, around 100–150 °C, the *PBIM* is not operated in that temperature. Moreover, since the cells are used in a PV system, the discharge rate is relatively low (less than 1C). Therefore, the capacity fading at high current rates will not affect the *PBIM*. For LFP, the most significant disadvantage is the low average voltage which results in low energy. However, this cell still has a superior energy density compared to other cathode materials [25].

Moreover, for the *PBIM*, the form factor (geometry of the cell) is also relevant as prismatic and pouch cells can help to achieve higher capacity per unit of volume than cylindrical cells. Therefore, cells with these form factors (pouch and prismatic) were chosen for the study.

Having identified LCO and LFP cells as potential battery technologies, the next section describes the causes behind battery aging and the influence of parameter such as current (related to C-rate), temperature, region of operation, and calendar aging.

2.2. Aging in Li-ion cells

The aging in electrochemical cells results in capacity fading which is referred to loss of available power or energy. The reduction of power in a battery is caused by an increase in the internal impedance, which then reduces the operating voltage of a cell. While the loss of the energy is a result of a change of the active material to inactive material [32], degradation or aging process includes a decrease in the battery's capacity and an increase of the battery resistance leading to a battery failure. This process can be created by the conditions at which the battery is operated. Unfortunately, the aging process in lithium-ion batteries is complex, since the cause of aging is caused by various interdependent mechanisms that cannot be studied separately [33].

Aging mechanisms can be divided into two categories, degradation produced by chemical reactions, and degradation caused by mechanical stress. Chemical degradation mechanisms consist of reduction and decomposition of the electrolyte, formation of solid-electrolyte interphase, binder decomposition, gas evolution, lithium-ion loss, and solvent co-intercalation [34]. The mechanical degradation of the battery mainly involves volume changes and stresses that occur in the active materials of the battery [35]. The volume changes and stresses can result in cracks, loss of contacts between active materials, and isolation [36]. These mechanisms can happen in different parts of a battery cell; the subsections below will compare different degradation modes that foster the battery aging in the anode, cathode, and separator.

2.2.1. C-rate

High discharge and charge currents could increase capacity fading rates. One possible cause is related to the change on carbon structure at high discharge current rates, leading to an electrolyte or salt reduction on the carbon surface due to the instability of the electrolyte. This reaction will produce gas and decomposition which will ultimately thicken the solid electrolyte interphase (SEI) on the carbon electrode. Furthermore, during a high current rate, the internal battery temperature augments, causing an increase in electrolyte reduction rate which produces gas increasing pressure, and damages the surface film [37].

2.2.2. Temperature

According to the Arrhenius law, the chemical reaction rate is proportional to the temperature. Therefore, an increase in temperature results in an exponential rise in electrochemical reaction rates. According to Ref. [35], a 10°C increment in temperature could double the degradation rate of a cell. At high temperature the protective SEI, formed at the first cells cycles, degrades faster, provoking the dissolution of SEI and propitiating the formation of more stable inorganic products such as lithium salts, e.g., lithium fluoride or lithium carbonate [33]. These new compounds are not just harder, which makes more difficult the Li-ion diffusion, but contribute to decrease the amount of active Li [38]. Hence, the capacity loss of the cell is the consequence.

2.2.3. Region of operation

The battery internal resistance increases when the cells are almost completely full or empty, which correlates with high SOCs and low SOCs, respectively. Therefore, cells that undergo processes in which the SOC varies significantly end up working in regions with high internal resistance. High internal resistance leads to a rise in battery temperature, which ultimately causes a faster capacity degradation rate.

2.2.4. Calendar aging

This type of aging is not related to the aging due to the activity of the battery, instead it has to do with the periods of battery inactivity. For instance, if the batteries are stored at high temperatures, that can help to accelerate the degradation of the battery [39]. Also, when cells are stored at high SOC levels, anode remains fully lithiated which result in an unstable electrode that could interact with the solvent components reducing the amount of electrode available [40].

3. Methodology for battery selection

The procedure followed to select a battery technology is summarized in Fig. 1a, where the process started by comparing the various technologies and filtering out the technologies that are not feasible in terms of suggested temperature of operation, complexity of implementation, form factor, and cost. This step was thoroughly carried out in Section 2, resulting in Li-ion cells as the technology that shows better features. Secondly, an integrated model, explained in more detail in the next section, was developed with two main objectives in mind: to evaluate battery technology candidates and help in the design of the testing experiment. The battery candidates will be evaluated employing a common tailor-made model that replicates the conditions of a PV-battery system. For the testing design, the model is useful to define the current profiles applied in the degradation testing and estimates the expected aging with a model previously published by the authors in Ref. [11]. Thirdly, the test not only includes the influence of the

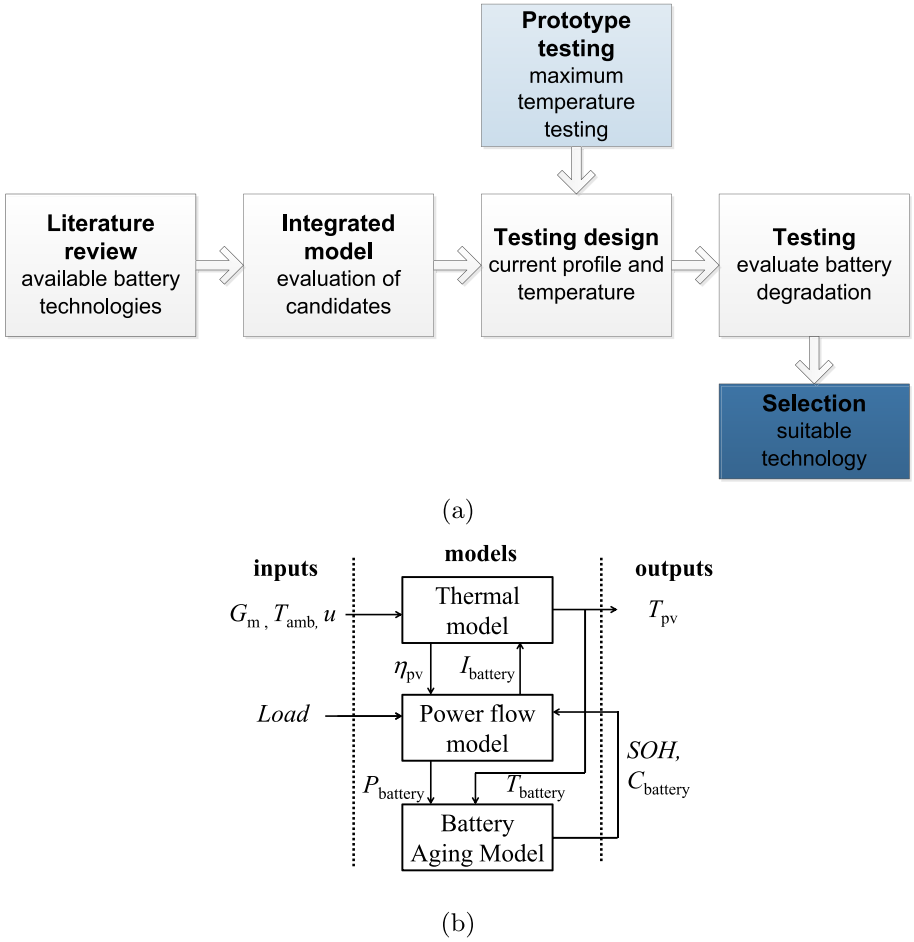

Fig. 1. (a) Methodology for selecting a suitable battery technology for the *PBIM*. It consists of a literature review, a integrated model, and a testing design which take as inputs the results of a prototype testing. Finally, the testing is carried out to propose the suitable battery technology, and (b) integrated model that includes power flow management, battery dynamic model, battery thermal model, and battery aging model.

charging and discharging profiles of a typical off-grid system but also takes into account the information provided by the prototype testing, which is used to set the maximum temperature of the degradation test [7].

Finally, once the cycling testing is set, the selected technology is extensively tested to quantify the effect of temperature and different current profiles on battery degradation. For comparison purposes, two sets of experiments were carried out simultaneously, one tries to follow the severe conditions defined by the prototype testing, and the second is controlled to reproduce the relatively low temperature of a typical PV system with the battery at a relatively constant temperature close to ambient. Based on these results, a battery technology is suggested to be more appropriate for the characteristics of the *PBIM*.

3.1. Integrated model

The integrated model is a combination of a 1-D thermal model previously introduced by the authors in Ref. [41], a battery aging model also product of the authors research [11], and power flow management model [42].

3.1.1. Inputs to integrated model

The steady state integrated model takes the solar irradiation, wind speed, and ambient temperature from a selected place in rural Cambodia, Strung Treng (13.517 °N, 105.967°E), for one year with 1 min time step, as reported in Ref. [42]. The load profile was selected from a previous paper that introduced a methodology to construct load profiles for based on the multi-tier framework for electricity access [43]. For the study undertaken in this article, the tier 3 load was used, and its profile can be observed in Fig. 2a. For this profile, the most prominent peak starts at night (18 h) because multiple appliances demand power at the same time, which coincide with activities such as lighting and cooking as all the members of the families return home.

The battery is charged during the day, and later the energy charged is discharged to provide energy in the night. In the night, the highest discharge currents are expected around the peak consumption times.

By utilizing the integrated model, three battery technologies, namely lead-acid, NiCd, and $LiFePO_4$, were studied; their main features can be observed in Table 2. Although the batteries in Table 2 are not necessarily suitable for the *PBIM*, they serve for the purpose of comparing battery technologies based on aging.

3.1.2. Interrelationship between individual models

The temperature of the battery, as well as the PV temperature, are calculated using a 1-D steady state thermal resistance model of the *PBIM* that allows the precise calculation of the PV efficiency and PV power [41].

The power flow model decides the direction and magnitude of the power delivered to the load according to the PV power production and battery state of charge as presented in Refs. [42,44].

Lastly, the temperature of the battery and energy processed by the battery are incorporated into a generic model that uses the relationship between cycles, depth of discharge (1-SOC), and temperature usually reported by battery manufacturers. This model is based on a zero

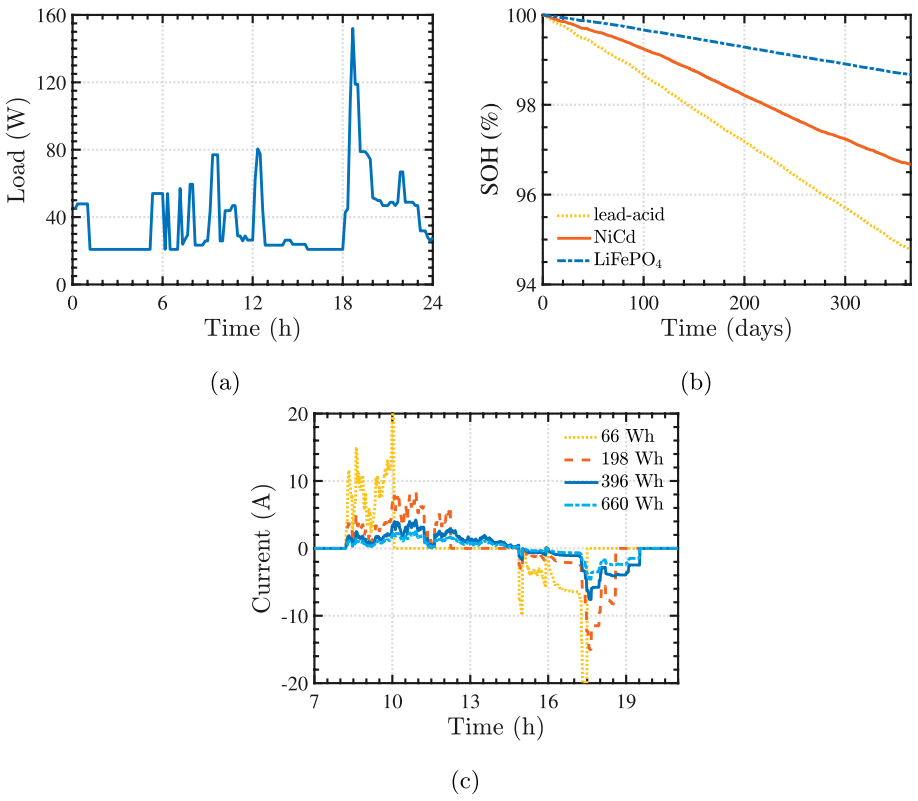

Fig. 2. (a) Tier 3 load profile (sourced from Ref. [43]), (b) state of health for three battery technologies after a year of simulation: LA, NiCd, and Li-ion, and (c) four current profiles for different battery sizes: 66 Wh, 198 Wh, 396 Wh, and 660 Wh.

Table 2
Specifications of three different battery types.

Technology	Brand	Capacity (Ah)	Voltage (V)
$LiFePO_4$	ValenceU1-12XP	10	3.2
Lead-acid (Sealed)	Enersys Cyclon D Single Cell	2.5	2.3
NiCd	Saft Nickel–Cadmium VRE D	5.5	1.2

crossings method that considers the degradation due to battery cycling every period of activity [11]. Consequently, the new capacity of the battery is determined and is fed back to the dynamic battery aging model; in this manner, the useable capacity of the battery continue decreasing as the simulation time advances.

In this integrated model, the individual models are merged into one that more realistically reproduces the conditions expected in the *PBIM*. From the model illustrated in Fig. 1b, it can be observed that the thermal model is interconnected to the power flow management model via the PV efficiency. The efficiency also defines the PV power output (P_{PV}) based on the temperature of the PV panel. Similarly, the current of the battery is needed to find the battery heat generation, which is fed to the thermal model. This process is iteratively repeated several times till the value T_{PV} and $T_{battery}$ does not vary more than 0.01 °C for every time step.

Once the iterative process between the thermal model and power management model has finished, the power needed from the battery ($P_{battery}$) and the temperature of the battery is used by the aging model to estimate the new capacity of the battery that is updated in the power management model for the next time step.

3.2. Results of the integrated model

After performing a simulation for one year, the state of charge for every battery is depicted in Fig. 2b. For all the cases, the battery size is 660 Wh (also referred as 10 batteries) and the PV rating 320 W_p. It can be observed that the lead-acid battery presents the lowest SOH followed by the NiCd which also degraded faster than the Li-ion battery. As a result, the focus of this paper will be on Li-ion batteries as they can last longer than other technologies in PV-battery systems.

Once Li-ion is chosen, the battery capacity is increased in steps of 66 Wh (1 battery), from 66 Wh to 660 Wh (10 batteries) to understand its effect on current profiles. As expected, less number of batteries connected in series, results in high instantaneous current values, as for the same power the voltage is lower, compared to bigger battery packs. This can be observed in Fig. 2c, where the green dashed line for 1 battery reaches values beyond 20 A, while for the other battery sizes the current never surpasses 10 A. The extension of the battery idle period also varies as a function of battery size, smaller battery sizes causes more extended inactivity periods.

3.3. Testing design

For the current profiles used in the testing, a cycle is considered as a complete charging discharging process; the charging happens in the day and the discharging starts in the afternoon and extends to the night. During these two processes, the battery is completely charged and fully discharged later, and the energy charged and discharged is identical. In terms of SOC, it is established that the battery SOC should never drop below 10% or be charged above 90%. This is defined to prevent over-discharging and overcharging.

Another important feature of the testing is that the periods of inactivity are eliminated with the objective of shortening the duration of each cycle, and therefore, be able to realize more than one cycle per natural day. The final profiles used in the testing are plotted in Fig. 3. Two profiles, 66 Wh and 198 Wh, were chosen as they represent the cases in which the battery pack experience the two highest current values. Here, it is important to point out that the energy processed by the battery in both cases (profiles) is the same, they just differ on the current

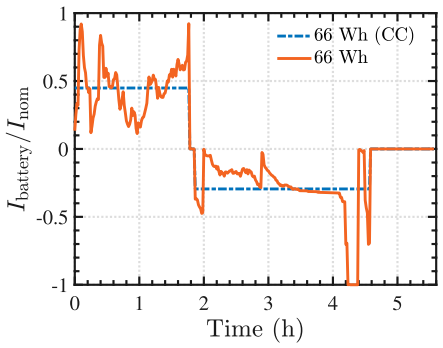

(a) For a battery size of 66 Wh, the dashed blue line corresponds to the CC profile and the red line to the dynamic profile.

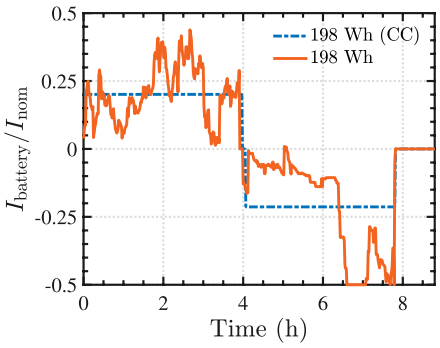

(b) For a battery size of 198 Wh, the dashed blue line corresponds to the CC profile and the red line to the dynamic profile.

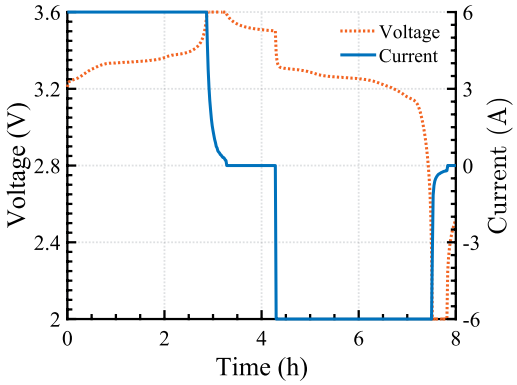

(c)

Fig. 3. Current profile for (a) 66 Wh battery size and (b) 198 Wh battery size, and (c) constant current and constant voltage profile for capacity measurement.

values and on the cycle duration. The purpose is, therefore, to investigate if dissimilar profiles result in different degradation rates. In Fig. 3a and b, a red dashed line can be noted; this line depicts the constant current (CC) equivalent profile associated to every battery size. The CC profiles are also added to investigate whether they speed up or reduce the battery aging rate in comparison to the dynamically changing profiles — they also cycle the same energy. In total, the 66 Wh profiles take 5.5 h to be executed, while the 198 Wh profile lasts for 10.83 h including the 5 min resting time between charging and discharging in both profiles to allow a brief voltage relaxation.

Battery temperature is recognized to have a significant influence on degradation. Therefore, two temperature extremes were defined in order to delimit the region in which the *PBIM* is expected to work. Consequently, as stated in Ref. [7], the upper limit reached by the batteries in poor cooling conditions and high irradiation was 45°C. Therefore, based on the prototype testing, the batteries will be tested at 45°C using the two previously commented profiles. Conversely, the cycling testing will be carried out at an ambient temperature varying between 22 and 26°C. This temperature range corresponds to the expected thermal response of a standard PV-battery system with the batteries placed indoors. In a previous paper by the authors, similar temperatures were measured [7].

With the objective of measuring the actual battery capacity after every cycling test, the procedure used consist of three main phases, a charging step composed of a CC and constant voltage (CV), a resting period of 1 h, and a discharging period with a CC-CV profile, as described in Fig. 3c.

After describing the formulation of the battery degradation test, the general procedure for the testing can be summarized as follows:

- **Cycling**: profiles that represented a battery size of 66 Wh and 198 Wh are repeated around 30 times and 20, respectively. After these repetitions, the battery capacity is measured as follows.
- **Capacity measurement**: the discharged capacity is measured and compared to the previous values at 25°C.
- **Charge to 10% SOC**: because the battery was completely discharged in the previous step, the battery must be charge till 10% so the cycling test can be resumed.

4. Battery testing set-up

According to Section 2.1, $LiFePO_4$ (LFP) and a $LiCoO_2$ (LCO) were selected to undergo the cycling test. In Table 3, the characteristics of the LFP and LCO batteries are presented; this information is fundamental for both the cycling current profiles and the capacity the measurement steps. Based on the nominal current, the magnitude of the current for all the time steps is determined accordingly. For instance, 18.44 A is the maximum current imposed to the LFP and 2.58 A for the LCO — for a battery size of 66 Wh. The end-of-discharge voltage and maximum voltage are set as the upper and lower values for the capacity measurement step; at these voltages, the transitions from CC to CV are defined for the charging and discharging processes. Moreover, because

Table 3
Technical specifications of A123 systems AMP20M1HD-A cell [45] and Renata ICP606168PRT cell [46].

Specifications	$LiFePO_4$	$LiCoO_2$
Nominal capacity	20 Ah	2.8
Nominal current	6 A	0.56
Nominal voltage	3.3 V	3.7
End-of-discharge voltage	2.0 V	3
Maximum voltage	3.6 V	4.2

the batteries are fully discharged after the capacity measurement, 10% of the capacity is charged at the nominal battery current given by the manufacturer. Here, it is important to clarify that the 10% SOC is updated after every capacity measurement to account for the battery degradation suffered.

A dynamic profile, as the name suggests, it is characterised by a constantly changing value of the current, while in a CC profile the value of the current is fixed for a predefined period. As an overview, Table 4 introduces the general arrangement of the testing. Eight LFP batteries (from LFP #1 to LFP #8) are tested at two reference temperatures, 45°C and 22–26°C (room temperature), and following four different current profiles, namely, dynamic 66 Wh (D66), 66 Wh at CC (CC66), dynamic 198 Wh (D198), and 198 Wh at CC (CC198).

For the four LCO cells, they were examined using two current profiles, dynamic 66 Wh and dynamic 198 Wh, for two temperatures, 45°C and 22–26°C, due to limitations in the number of channels available. The initial capacity of the cells is reported in Table 4, showing a slight difference among them.

4.1. Equipment

The general testing set-up is shown in Fig. 4a, where the climate chamber in charge of keeping the temperature at 45°C, the battery tester, and the chamber that maintains the batteries at room temperature can be seen. The climate chamber (Memmert, Climatic test chamber CTC 256) was able to sustain the temperature of the chamber within ±2°C from the set point.

Each cell had a K-type thermocouple attached to it to monitor its thermal behavior throughout the testing, as well as the voltage was continuously measured (Fig. 4b and c), the information was retrieved and saved by the battery tester every 1 min.

The battery tester (Arbin, model LBT22043) has 16 channels and the maximum absolute current that can be drawn from a single channel is 10 A (Table 5). For these reasons, channels 1&2 and 6&7 are connected in parallel so they can provide current beyond 10 A as requested by 66 Wh profile for the LFP cell. Finally, the batteries placed inside the climate chamber present slight differences in temperature due to the not completely uniform temperature distribution inside the climate chamber; however, the difference between them was never more than 1.5°C.

Table 4
Initial capacities for the selected cells.

Channel	Battery	Profile	Temperature (°C)	Initial capacity (Ah)
1,2	LFP #1	D66	45	20.06
3	LFP #2	CC66	45	20.02
4	LFP #3	D198	45	19.90
5	LFP #4	CC198	45	20.05
6,7	LFP #5	D66	RT	20.10
8	LFP #6	CC66	RT	20.28
9	LFP #7	D198	RT	19.83
10	LFP #8	CC198	RT	20.39
11	LCO #1	D66	45	2.73
12	LCO #2	D198	45	2.78
13	LCO #3	D66	RT	2.71
14	LCO #4	D198	RT	2.75

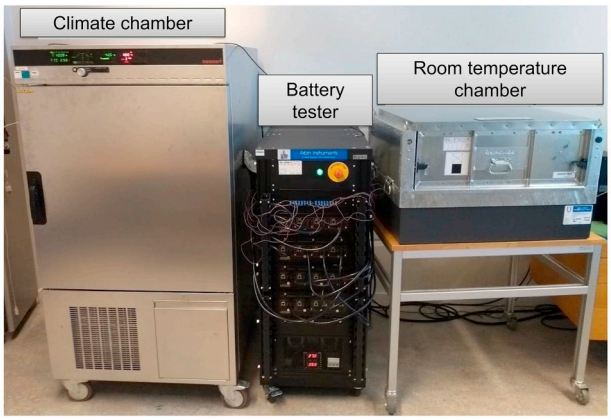

(a) General set-up

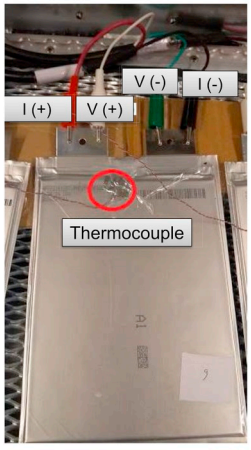

(b) LFP

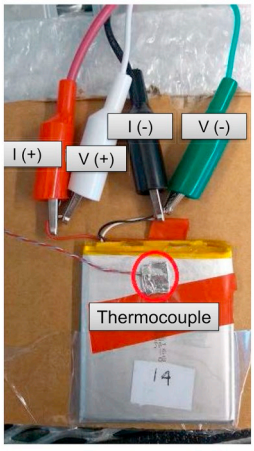

(c) LCO

Fig. 4. (a) General set-up consisting of a climate chamber, a battery tester, and chamber at room temperature. (b) Interconnection and location of thermocouple for a chose LFP cell. (c) Interconnection and location of thermocouple for a chosen LCO cell.

Table 5
Technical specifications of the battery tester Arbin, model LBT22043.

Specifications	Value
Number of test channels	16 channels
Voltage ranges	0–25 V
Current ranges	−10–10 A
Temperature ranges	0–100°C
Operating modes	CC, CV, and CC-CV

5. Battery degradation results

In this section, the effect of temperature and the different current profiles over battery degradation are analyzed for the $LiFePO_4$ and $LiCoO_2$ cells. Also, a comparison between these two technologies is carried out to select the most suitable one. Here, it is important to point out that for the 66 Wh profile, more cycles were performed because it lasts shorter than the 198 Wh profile; however, when analyzing the results between current profiles, the values are interpolated to perform a fair comparison.

5.1. Lithium iron phosphate cells

5.1.1. Temperature effect

As anticipated, the batteries tested at 45°C presented lower SOH

values compared to the batteries maintained at room temperature for the same current profiles (Fig. 5a and Fig. 5b). Although in general high temperatures cause an immediate increase in the ability of the battery to store and release energy, the capacity of the battery tends to decrease faster in the long term relative to batteries exposed to colder conditions. Because the chemical activity is incentivized by warm conditions, the electrochemical reactions increase their rates favoring the intercalation process but also provoking a faster consumption of active lithium by means of undesired side reactions.

In Fig. 5a, it can be seen that the degradation is more pronounced as the batteries are more cycled for both the CC profile and the dynamic profiles. To quantify this change, Table 6 summarizes the results for the LFP cells cycled with 66 Wh profiles. The difference between the cells cycled at 25°C and 45°C in SOH was 0.77%, 1.68%, and 1.84% for the cycles 100, 190, and 250, respectively showing an increasing trend. Similarly, for the CC profile, the LFP cells degraded 1.64% less at 25°C than at 45°C in the cycle number 250. In Fig. 5b and Table 7, the same behavior is observed for the 198 Wh profile.

5.1.2. Comparing between constant current (CC) dynamic profile

In this section, the consequences of imposing a CC or dynamic current profiles are analyzed for the same temperatures. This is done for the profiles corresponding to a battery size of 66 Wh and 198 Wh. The results are summarized in Tables 6 and 7

When comparing the D66 profile and the CC66 profile at 45°C, it can be observed that the SOH is always higher in the case of the CC profile (Table 6). For instance, at the cycle 250, the difference in terms of SOH varies from 0.2 to 0.9% for all the cycles (0–250). For the 66 Wh profile, now at room temperature, the CC profile sometimes results in higher SOHs while for other cycles is lower, as depicted in Fig. 5a, but the differences are always within ±0.35%. Therefore, it can be said that the CC profile at 45°C presents lower degradation than the dynamic profile, but at 25°C no representative trend is observed.

When having a look at the 198 Wh battery size (Fig. 5b and Table 7), two main conclusions can be drawn: the CC profile presents the lower SOH at 45°C, and for room temperature, a slight positive effect of CC can be seen.

If a general observation were to be made about the positive or negative effect of imposing a CC profile over the LFP cells, more extensive testing must be performed to elucidate the causes of the contradictory information observed for the 66 Wh and 198 Wh sizes.

5.1.3. Comparing profiles with different battery sizes for LFP: 66 Wh vs. 198 Wh

This section explores the relationship between the current profiles defined for the 66 Wh and 198 Wh battery sizes not considering the influence of temperature. By using Table 8, the profiles can be studied based on the difference of SOH after 51, 100, and 160 cycles.

Table 6
Difference in SOH (ΔSOH) between cells tested at RT and 45°C for LFP cells after 100, 190 and 250 cycles. The cells are cycled with a constant current profile (CC66) and a dynamic profiles (D66) for a battery size of 66 Wh.

cycles	SOH (%) 45°C	SOH (%) 25°C	Δ SOH (%)	SOH (%) 45°C (CC)	SOH (%) 25°C (CC)	Δ SOH (%)
100	98.59	99.35	0.77	98.79	99.35	0.56
190	97.18	98.86	1.68	98.08	98.88	0.79
250	96.51	98.35	1.84	97.06	98.70	1.64

Table 7
Difference in state health (ΔSOH) between cells tested at RT and 45°C for LFP cells after 46, 102 and 160 cycles. The cells are cycled with a constant current profile (CC198) and a dynamic profiles (D198) for a battery size of 198 Wh.

cycles	SOH (%) 45°C	SOH (%) 25°C	Δ SOH (%)	SOH (%) 45°C (CC)	SOH (%) 25°C (CC)	Δ SOH (%)
46	99.67	99.86	0.18	98.92	99.78	0.86
102	98.41	99.10	0.68	97.84	99.24	1.41
160	97.56	98.70	1.14	97.20	98.85	1.65

By keeping the temperature value at 45°C and contrasting the SOHs for the 66 Wh and 198 Wh dynamic profiles, there is no a clear indication about the effect of the profiles on battery degradation as the dissimilarity between them is not more than 0.25% for any cycle. Similarly, at 25°C, the SOH remains slightly higher in favor of the 66 Wh profile with a maximum difference of 0.3%. Thus, it is concluded that the effect of the momentously higher currents experienced in the 66 Wh profile compared to the longer cycles are not more harmful than the more extended profiles defined for the 198 Wh current profiles.

5.1.4. Which parameter plays a more prominent role for the LFP cells?

From Section 5.1.1, differences till 1.84% on SOH were found for

Table 8
Difference in SOH (ΔSOH) for cells tested using profiles representing the battery sizes of 66 Wh and 198 Wh for LFP cells after 51, 100 and 160 cycles. The cells were tested at 45°C and room temperature. Note: the values for 198 Wh were linearly interpolated to make a fair comparison between battery sizes. For cycle 51: 46–64, and for cycle 100: 83–102.

cycles	SOH (%) 45°C, 66 Wh	SOH (%) 45°C, 198 Wh	Δ SOH (%)	SOH (%) 25°C, 66 Wh	SOH (%) 25°C, 198 Wh	Δ SOH (%)
51	99.78	99.54	0.25	99.97	99.77	0.20
100	98.59	98.46	0.13	99.35	99.12	0.23
160	97.47	96.56	−0.09	99.00	98.70	0.3

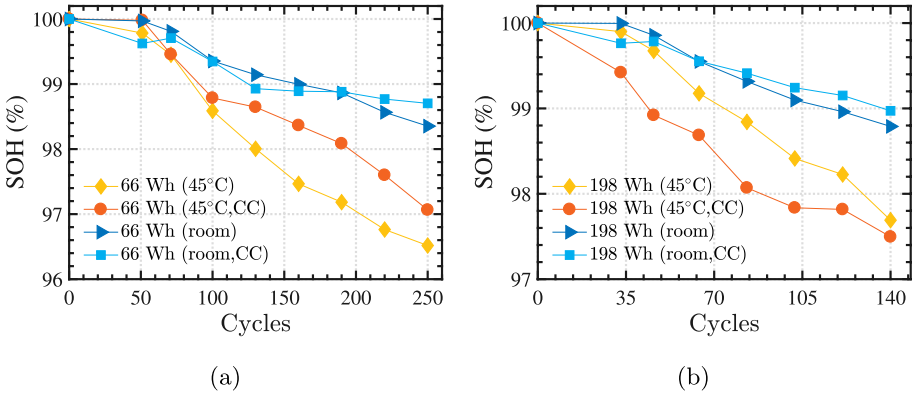

Fig. 5. (a) LFP cells cycled with a dynamic 66 Wh profile (D66) at room temperature and 45°C, and (b) LFP cells cycled with a dynamic 198 Wh profile (D198) at room temperature and 45°C.

batteries exposed to 45°C, while using a CC compared to dynamic profiles does not show a definitive negative impact on battery aging. Moreover, the different current profiles corresponding to battery sizes of 66 Wh and 198 Wh seem not to cause a significant adverse impact on battery aging. Therefore, the negative influence of high temperature is the primary cause behind the accelerated degradation for the LFP cells tested.

5.2. Lithium cobalt oxide cells

For the LCO cells, just the impact of two temperatures and two different current profiles — dynamic 66 Wh and dynamic 198 Wh — were investigated. The relationship between capacity fading and cycling are illustrated by Fig. 6a and b. A general feature can be observed for all the LCO cells, they presented a sharp drop in capacity at the beginning of the test, but as the cycling continued the capacity degradation rate decreased irrespectively of the current profile or testing temperature.

5.2.1. Comparing profiles with different battery sizes for LCO: 66 Wh vs. 198 Wh

Table 9 introduces the SOH for the D198 and D66 profiles along with the temperatures at which the experiments were performed. If the temperature is kept at 45°C, and the D66 profile is compared to the D198 profile, it can be found that the D198 results in almost a difference of 1% SOH with respect to the D66. Although as the cycling continues the difference between them reduces to only 0.25% SOH after 125 cycles. When the testing is completed at room temperature, the measurements show a no representative difference of 0.04% more SOH for the 66 Wh profile related to the 198 Wh profile. Hence, similarly to the conclusion reached in Section 5.1.3, the 66 Wh and 198 Wh current profiles do not have distinguishable effect on aging of the cells.

5.2.2. Temperature effect

The same behavior, observed for the LFP cells, where cycling the battery at 45°C caused a more accelerated degradation than batteries exposed to room temperature, also applies to the LCO cells. Based on Table 9, the capacity of the LCO cells faded by 1.53% and 1.23% of SOH for the D66 and D198 profiles, respectively. Furthermore, as the cycling advanced, there is a tendency to increase more the differences on SOH for the two temperature levels (refer to Fig. 6a and b).

5.3. Selecting a battery technology

As stated previously, the LFP and LCO were the chosen Li-ion cells to be tested in order to select one out of the two as the candidate for the *PBIM*. According to the aging test that both technologies underwent, the LFP cells present lower values of degradation, or higher SOHs, under the same testing conditions, for identically normalized current profiles and reference temperatures. Fig. 7 shows the SOH change as a function of the number of cycles for the 66 Wh and 198 Wh profiles. In the case of the 66 Wh profile for 45°C, there is a difference on SOH of 2.53% at the last cycle (130) in favor of the LFP cells. Similarly, for the 198 Wh profile, the LFP outperforms the LCO by 2.43% at 45°C. When analyzing the data obtained at room temperature, the reduction on SOH values are not as pronounced as for the 45°C; however, the same tendency remains, LFP aged slower. Therefore, LFP is selected as the battery technology to be used in the *PBIM* based on the capacity fading results.

Table 9
Difference in SOH (ΔSOH) between cells tested at 25 and 45°C for LCO cells after 25, 74, and 125 cycles. The cells are cycled with a dynamic 66 Wh and a dynamic 198 Wh profile.

cycles	SOH (%) 45°C, 66 Wh	SOH (%) 25°C, 66 Wh	Δ SOH (%)	SOH (%) 45°C, 198 Wh	SOH (%) 25°C, 198 Wh	Δ SOH (%)
25	96.35	97.79	1.44	97.34	97.53	0.19
74	96.11	97.44	1.33	96.27	96.99	0.72
125	95.46	96.99	1.53	95.71	96.95	1.23

5.4. Expected battery aging for PBIM

Assuming that the *PBIM* will operate for battery sizes that entail lower C-rates that the expected in the 66 Wh profile, the 198 Wh dynamic profile is chosen in this section to indicate the predicted aging for the *PBIM* considering its region of operation, while an estimation of the battery lifetime is calculated for this profile (198 Wh).

As presented in Fig. 8, the *PBIM* is expected to operate between the limits defined by the lower boundary (45°C) and the upper limit (room temperature), this in terms of degradation level. Because the maximum operating point determined by testing the *PBIM* prototype was 45°C in severe conditions, this condition is not likely to occur frequently. On the other hand, having the batteries operating as they were placed indoors is considered optimistic. As a consequence, the degradation of the batteries packed inside the *PBIM* is likely to occur between the boundaries proposed in Fig. 8.

5.5. Future research

The objective of the research presented in this paper was to select a suitable battery technology for the *PBIM*, however, more attention can be paid to the influence of charging/discharging profiles. For this purpose, a more extensive testing could be performed until the end-of-life of the batteries.

6. Conclusion

In this paper, a framework to select a suitable battery technology for

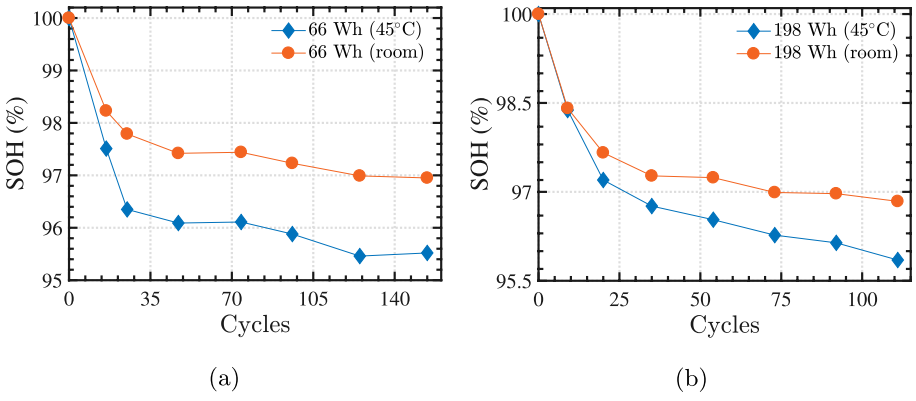

Fig. 6. (a) LCO cells cycled with a 66 Wh profile at room temperature and 45°C, and (b) LCO cells cycled with a 198 Wh profile at room temperature and 45°C.

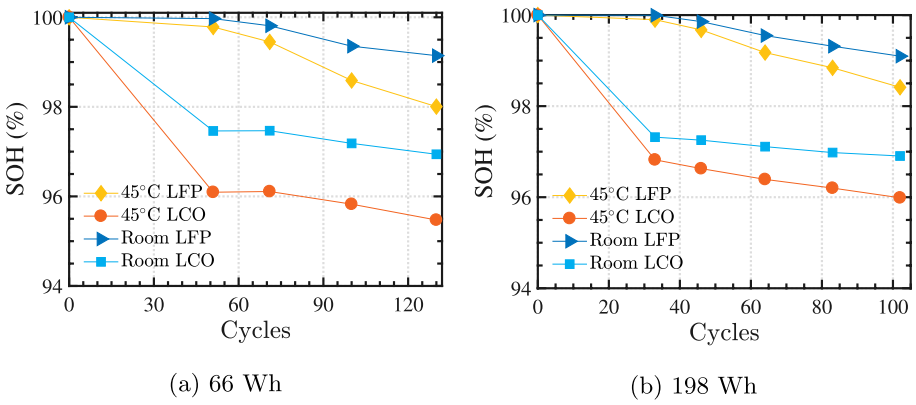

Fig. 7. Comparison of LFP and LCO for the (a) 66 Wh and (b) 198 Wh current profiles.

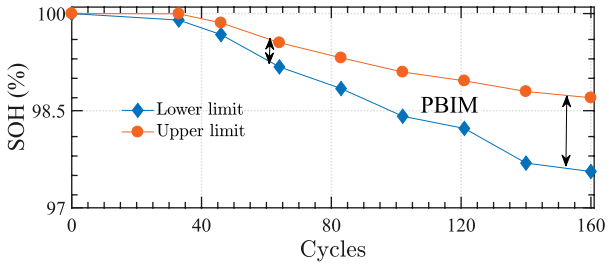

Fig. 8. Expected range of operation for *PBIM*.

the *PV-battery integrated module* is presented. The framework consisted of a literature review to select battery candidates among the available battery technologies, an integrated model to emulate operating conditions of the battery pack, an application-based testing design, and finally, an extended battery aging testing. Firstly, the literature review together with the use of the integrated model, helped identifying Li-ion cells as the most appropriate. Secondly, the testing was designed taking into account previous research done by testing a prototype, and also was constructed based on an integrated model that provides information about the typical current profiles expected for the *PBIM*. These current profiles were applied to the two selected Li-ion cells, namely $LiFePO_4$ and $LiCoO_2$, after a careful analysis of the available cells in the market. From the cycling testing results, it was found that the effect of high temperature is more significant than the influences of the applied current profiles on both types of cells. Between these two Li-ion chemistries, the $LiFePO_4$ present lower capacity fading rates, and as a consequence, it is suggested as the most suitable for the *PBIM*. Moreover, the expected range of degradation for a $LiFePO_4$ battery pack in the *PBIM* was reported. In conclusion, this paper provides a structure methodology to select a battery technology, and proves that the battery pack can perform appropriately when integrated at the back of a solar panel.

Acknowledgment

The authors thank Joris Koeners, Harrie Olsthoorn, and Bart Roodenburg for their help during the aging testing. The authors also thank the financial support of the Universidad de Costa Rica, Ministerio de Ciencia y Tecnología y Telecomunicaciones de Costa Rica, and Consejo Nacional para Investigaciones Científicas y Tecnológicas.

References

[1] Renewable Energy Sources and Climate Change Mitigation: Special Report of the Intergovernmental Panel on Climate Change, Cambridge University Press, 2011, https://doi.org/10.1017/CBO9781139151153.
[2] I.E. Agency, Technology Roadmap Solar Photovoltaic Energy, 2014.
[3] J.F. Reynaud, C. Alonso, P. Aloisi, C. Cabal, B. Estibals, G. Rigobert, G. Sarre, H. Rouault, D. Mourzagh, F. Mattera, S. Genies, Multifunctional module lithium-ion storage and photovoltaic conversion of solar energy, in: Conference Record of the IEEE Photovoltaic Specialists Conference, 2008, pp. 1–5.
[4] W. Grzesiak, P. Mackow, T. Maj, A. Polak, E. Klugmann-Radziemska, S. Zawora, K. Drabczyk, S. Gulkowski, P. Grzesiak, Innovative system for energy collection and management integrated within a photovoltaic module, Sol. Energy 132 (2016) 442–452, https://doi.org/10.1016/j.solener.2016.03.043.
[5] V. Vega-Garita, D.D. Lucia, N. Narayan, L. Ramirez-Elizondo, P. Bauer, Integrating a photovoltaic storage system in one device: a critical review, Prog. Photovolt. Res. Appl. (2018) 1–25.
[6] V. Vega-Garita, L. Ramirez-Elizondo, P. Bauer, Physical integration of a photovoltaic-battery system: a thermal analysis, Appl. Energy 208 (2017) 446–455, https://doi.org/10.1016/j.apenergy.2017.10.007. September.
[7] V. Vega-Garita, S. Garg, N. Narayan, L. Ramirez-Elizondo, P. Bauer, Testing a pv-battery integrated module prototype, in: IEEE 7th World Conference on Photovoltaic Energy Conversion, vol. 2018, WCPEC, 2018, pp. 1244–1248, https://doi.org/10.1109/PVSC.2018.8548111.
[8] G.J. May, A. Davidson, B. Monahov, Lead batteries for utility energy storage: a review, J. Energy Storage 15 (2018) 145–157. https://doi.org/10.1016/j.est.2017.11.008.
[9] M. Sufyan, N.A. Rahim, M.M. Aman, C.K. Tan, S.R.S. Raihan, Sizing and applications of battery energy storage technologies in smart grid system: a review, J. Renew. Sustain. Energy 11 (1) (2019) 014105, https://doi.org/10.1063/1.5063866.
[10] D. Parra, M. Gillott, S.A. Norman, G.S. Walker, Optimum community energy storage system for pv energy time-shift, Appl. Energy 137 (2015) 576–587. https://doi.org/10.1016/j.apenergy.2014.08.060.
[11] N. Narayan, T. Papakosta, V. Vega-Garita, Z. Qin, J. Popovic-Gerber, P. Bauer, M. Zeman, Estimating battery lifetimes in solar home system design using a practical modelling methodology, Appl. Energy 228 (2018) 1629–1639. https://doi.org/10.1016/j.apenergy.2018.06.152.
[12] C. Zhang, Y.-L. Wei, P.-F. Cao, M.-C. Lin, Energy storage system: current studies on batteries and power condition system, Renew. Sustain. Energy Rev. 82 (2018) 3091–3106. https://doi.org/10.1016/j.rser.2017.10.030.
[13] M. Freitas, T. Penha, S. Sirtoli, Chemical and electrochemical recycling of the negative electrodes from spent, NiCd Batter. 163 (2) (2007) 1114–1119, https://doi.org/10.1016/j.jpowsour.2006.09.087.
[14] P. Bernard, M. Lippert, NickelCadmium and NickelMetal Hydride Battery Energy Storage, vol. 223, 2015, https://doi.org/10.1016/B978-0-444-62616-5.00014-0.
[15] C. Nogueira, F. Margarido, Chemical and physical characterization of electrode materials of spent sealed NiCd batteries, Waste Manag. 27 (11) (2007) 1570–1579, https://doi.org/10.1016/j.wasman.2006.10.007.
[16] X. Hu, C. Zou, C. Zhang, Y. Li, Technological developments in batteries: a survey of principal roles, types, and management needs, IEEE Power Energy Mag. 15 (5) (2017) 20–31.
[17] N. Omar, Y. Firouz, M. Monem, A. Samba, H. Gualous, T. Coosemans, P.V. den Bossche, J.V. Mierlo, Analysis of nickel-based battery technologies for hybrid and electric vehicles, in: Reference Module in Chemistry, Molecular Sciences and Chemical Engineering, Elsevier, 2014. https://doi.org/10.1016/B978-0-12-409547-2.10740-1.
[18] X. Hu, C. Zou, C. Zhang, Y. Li, Technological developments in batteries: a survey of principal roles, types, and management needs, IEEE Power Energy Mag.:10.1109/MPE.2017.2708812.
[19] A. Poullikkas, A comparative overview of large-scale battery systems for electricity storage, Renew. Sustain. Energy Rev. 27 (2013) 778–788, https://doi.org/10.1016/j.rser.2013.07.017.
[20] M. Skyllas-Kazacos, J.F. Mccann, Vanadium redox flow batteries (VRBs) for medium- and large-scale energy storage, in: Advances in Batteries for Medium and Large-Scale Energy Storage, vol. 329, 2015, https://doi.org/10.1016/B978-1-78242-013-2.00010-8.
[21] M. Wild, L. O'Neill, T. Zhang, R. Purkayastha, G. Minton, M. Marinescu, G. J. Offer, Lithium sulfur batteries, a mechanistic review, Energy Environ. Sci.doi:10.1039/C5EE01388G.

[22] L. Yue, J. Ma, J. Zhang, J. Zhao, S. Dong, Z. Liu, G. Cui, L. Chen, All solid-state polymer electrolytes for high-performance lithium ion batteries, Energy Storage Mater. 5 (2016) 139–164. https://doi.org/10.1016/j.ensm.2016.07.003.
[23] J.G. Kim, B. Son, S. Mukherjee, N. Schuppert, A. Bates, O. Kwon, M.J. Choi, H. Y. Chung, S. Park, A review of lithium and non-lithium based solid state batteries, J. Power Sources 282 (2015) 299–322. https://doi.org/10.1016/j.jpowsour.2015.02.054.
[24] J.W. Fergus, Recent developments in cathode materials for lithium ion batteries, J. Power Sources 195 (4) (2010) 939–954.
[25] G. Berckmans, M. Messagie, J. Smekens, N. Omar, L. Vanhaverbeke, J. Van Mierlo, Cost projection of state of the art lithium-ion batteries for electric vehicles up to 2030, Energies 10 (9). doi:10.3390/en10091314.
[26] N. Nitta, F. Wu, J.T. Lee, G. Yushin, Li-ion battery materials: present and future, Mater. Today 18 (5) (2015) 252–264, https://doi.org/10.1016/j.mattod.2014.10.040, arXiv:arXiv:1011.1669v3.
[27] D.H. Doughty, E.P. Roth, A general discussion of li ion battery safety, Electrochem. Soc. Interface 21 (2) (2012) 37–44, https://doi.org/10.1149/2.F03122if.
[28] P. Kalyani, N. Kalaiselvi, Various aspects of LiNiO2 chemistry: a review, Sci. Technol. Adv. Mater. 6 (6) (2005) 689–703, https://doi.org/10.1016/j.stam.2005.06.001.
[29] C. Chen, J. Liu, M. Stoll, G. Henriksen, D. Vissers, K. Amine, Aluminum-doped lithium nickel cobalt oxide electrodes for high-power lithium-ion batteries, J. Power Sources 128 (2) (2004) 278–285. https://doi.org/10.1016/j.jpowsour.2003.10.009.
[30] L. Yunjian, L. Xinhai, G. Huajun, W. Zhixing, H. Qiyang, P. Wenjie, Y. Yong, Electrochemical performance and capacity fading reason of LiMn2O4/graphite batteries stored at room temperature, J. Power Sources 189 (1) (2009) 721–725, https://doi.org/10.1016/J.JPOWSOUR.2008.08.044.
[31] N. Yabuuchi, T. Ohzuku, Novel lithium insertion material of LiCo1/3Ni1/3Mn1/3O2 for advanced lithium-ion batteries, J. Power Sources (2003), https://doi.org/10.1016/S0378-7753(03)00173-3.
[32] T.M. Bandhauer, S. Garimella, T.F. Fuller, A critical review of thermal issues in lithium-ion batteries, J. Electrochem. Soc. 158 (3) (2011) R1, https://doi.org/10.1149/1.3515880.
[33] J. Vetter, P. Novák, M.R. Wagner, C. Veit, K.C. Möller, J.O. Besenhard, M. Winter, M. Wohlfahrt-Mehrens, C. Vogler, A. Hammouche, Ageing mechanisms in lithium-ion batteries, J. Power Sources 147 (1–2) (2005) 269–281, https://doi.org/10.1016/j.jpowsour.2005.01.006.
[34] D.E. Demirocak, B. Bhushan, Probing the aging effects on nanomechanical properties of a lifepo4 cathode in a large format prismatic cell, J. Power Sources 280 (2015) 256–262. https://doi.org/10.1016/j.jpowsour.2015.01.114.
[35] M.M. Kabir, D.E. Demirocak, Degradation mechanisms in li-ion batteries: a state-of-the-art review, Int. J. Energy Res 41 (14) (2017) 1963–1986, https://doi.org/10.1002/er.3762. Int. J. Energy Res. 41 (14) 1963-1986. arXiv, https://onlinelibrary.wiley.com/doi/pdf/10.1002/er.3762.
[36] A. Mukhopadhyay, B.W. Sheldon, Deformation and stress in electrode materials for li-ion batteries, Prog. Mater. Sci. 63 (2014) 58–116. https://doi.org/10.1016/j.pmatsci.2014.02.001.
[37] G. Ning, B. Haran, B.N. Popov, Capacity fade study of lithium-ion batteries cycled at high discharge rates, J. Power Sources 117 (1–2) (2003) 160–169, https://doi.org/10.1016/S0378-7753(03)00029-6.
[38] R. Yazami, Y.F. Reynier, Mechanism of self-discharge in graphitelithium anode, Electrochim. Acta 47 (8) (2002) 1217–1223. https://doi.org/10.1016/S0013-4686(01)00827-1.
[39] P. Keil, S.F. Schuster, J. Wilhelm, J. Travi, A. Hauser, R.C. Karl, A. Jossen, Calendar aging of lithium-ion batteries, J. Electrochem. Soc. 163 (9) (2016) A1872–A1880, https://doi.org/10.1149/2.0411609jes.
[40] S. Grolleau, A. Delaille, H. Gualous, P. Gyan, R. Revel, J. Bernard, E. Redondo-Iglesias, J. Peter, Calendar aging of commercial graphite/LiFePO4cell - predicting capacity fade under time dependent storage conditions, J. Power Sources 255 (2014) 450–458, https://doi.org/10.1016/j.jpowsour.2013.11.098.
[41] V. Vega-Garita, A. P. Harsarapama, L. Ramirez-Elizondo, P. Bauer, Physical Integration of PV-Battery System: Advantages, Challenges, and Thermal Modeldoi: 10.1109/ENERGYCON.2016.7514038.
[42] V. Vega-Garita, D.D. Lucia, N. Narayan, L. Ramirez-Elizondo, P. Bauer, Pv-battery integrated module as a solution for off-grid applications in the developing world, in: IEEE International Energy Conference (ENERGYCON), vol. 2018, 2018, pp. 1–6.
[43] N. Narayan, Z. Qin, J. Popovic-Gerber, J.-C. Diehl, P. Bauer, M. Zeman, Stochastic load profile construction for the multi-tier framework for household electricity access using off-grid dc appliances, Energy Effic.doi:10.1007/s12053-018-9725-6.
[44] V. Vega-Garita, M. Sofyan, N. Narayan, L. Ramirez-Elizondo, P. Bauer, V. Vega-Garita, M.F. Sofyan, N. Narayan, L. Ramirez-Elizondo, P. Bauer, Energy management system for the photovoltaic battery integrated module, Energies 11 (12) (2018) 3371, https://doi.org/10.3390/en11123371.
[45] A123 Systems, Battery Pack Design, Validation, and Assembly Guide Using A123 Systems AMP20M1HD-A Nanophosphate Cells, 2014.
[46] S.A. Renata, Switzerland, Renata ICP606168PRT Engineering Specification, 2013.